Estimation of interval anisotropy parameters using velocity-independent layer stripping

Xiaoxiang Wang[1] and Ilya Tsvankin[1]

ABSTRACT

Moveout analysis of long-spread P-wave data is widely used to estimate the key time-processing parameter η in layered transversely isotropic media with a vertical symmetry axis (VTI). Inversion for interval η values, however, suffers from instability caused by the trade-off between the effective moveout parameters and by subsequent error amplification during Dix-type layer stripping. We propose an alternative approach to nonhyperbolic moveout inversion based on the velocity-independent layer-stripping (VILS) method of Dewangan and Tsvankin. Also, we develop the 3D version of VILS and apply it to interval parameter estimation in orthorhombic media using wide-azimuth, long-spread data. If the overburden is laterally homogeneous and has a horizontal symmetry plane, VILS produces the exact interval traveltime-offset function in the target layer without knowledge of the velocity field. Hence, Dix-type differentiation of moveout parameters used in existing techniques is replaced by the much more stable layer stripping of reflection traveltimes. The interval traveltimes are then inverted for the moveout parameters using the single-layer nonhyperbolic moveout equation. The superior accuracy and stability of the algorithm are illustrated on ray-traced synthetic data for typical VTI and orthorhombic models. Even small correlated noise in reflection traveltimes causes substantial distortions in the interval η values computed by conventional Dix-type differentiation. In contrast, the output of VILS is insensitive to mild correlated traveltime errors. The algorithm is also tested on wide-azimuth P-wave reflection data recorded above a fractured reservoir at Rulison field in Colorado. The interval moveout parameters estimated by VILS in the shale layer above the reservoir are more plausible and less influenced by noise than those obtained by the Dix-type method.

INTRODUCTION

Traveltime analysis of surface reflection data yields effective moveout parameters for the whole section above the reflector. However, for migration velocity analysis, amplitude-variation-with-offset (AVO) inversion, and seismic fracture characterization, one must obtain the interval properties of a target layer. Most existing approaches to interval parameter estimation, in both isotropic and anisotropic media, are based on layer stripping (e.g., Dix, 1955; Grechka and Tsvankin, 1998; Grechka et al., 1999) or tomographic inversion (e.g., Stork, 1992; Grechka et al., 2002).

The conventional Dix (1955) equation, derived for horizontally layered isotropic media, helps compute the interval normal-moveout (NMO) velocity using the NMO velocities for the reflections from the top and bottom of a layer. The Dix equation remains valid for horizontally layered VTI media; also, it is generalized by Alkhalifah and Tsvankin (1995) for dipping reflectors overlain by a laterally homogeneous VTI overburden. For 3D wide-azimuth data from layered azimuthally anisotropic media, the effective NMO velocity can be obtained by Dix-type averaging of the interval NMO ellipses (Grechka et al., 1999).

Unfortunately, NMO velocity often is insufficient to build the velocity field for anisotropic media, even in the time domain. This explains the importance of using nonhyperbolic (long-spread) reflection moveout in estimating anisotropy parameters. The P-wave long-spread reflection moveout in a horizontal VTI layer can be described by the following nonhyperbolic equation (Alkhalifah and Tsvankin, 1995; Tsvankin, 2005):

$$t^2 = t_0^2 + \frac{x^2}{V_{\text{nmo}}^2} - \frac{2\eta x^4}{V_{\text{nmo}}^2 [t_0^2 V_{\text{nmo}}^2 + (1 + 2\eta) x^2]}, \quad (1)$$

where x is the offset, t_0 is the two-way zero-offset reflection traveltime, V_{nmo} is the NMO velocity that controls the conventional-spread

---

reflection moveout of horizontal P-wave events, and η is the anellipticity coefficient responsible for the deviation from hyperbolic moveout at long offsets. For stratified VTI media, the moveout parameters become effective quantities for the stack of layers above the reflector. Many implementations of nonhyperbolic moveout inversion for VTI media (e.g., Alkhalifah, 1997; Grechka and Tsvankin, 1998; Toldi et al., 1999) are based on equation 1, which represents a simplified version of the more general Tsvankin-Thomsen (1994) equation. Accurate estimation of V_{nmo} and η makes it possible to carry out all P-wave time-domain processing steps, which include NMO and dip-moveout (DMO) corrections and time migration.

An alternative algorithm for η estimation operates with the dip dependence of P-wave NMO velocity (Alkhalifah and Tsvankin, 1995). Although the DMO inversion is relatively stable, its application is more complicated and requires the presence of dipping reflectors under the formation of interest (Tsvankin, 2005).

Nonhyperbolic moveout inversion for the parameters V_{nmo} and η usually involves a 2D semblance scan on long-spread data (the maximum offset should reach two reflector depths) from a horizontal reflector. Despite its relative simplicity, this method suffers from instability caused by the trade-off between V_{nmo} and η (Alkhalifah, 1997; Grechka and Tsvankin, 1998). Grechka and Tsvankin (1998) find that even small traveltime errors, which could be considered as insignificant in data processing, may cause large errors in η. For layered media, this error is amplified in the layer-stripping process, which may cause unacceptable distortions in the interval η values. The effective η function is often smoothed prior to applying the Dix-type equations, but smoothing does not remove the source of instability in the interval η estimation.

The Alkhalifah-Tsvankin (1995) equation has been extended to wide-azimuth data by taking into account the azimuthal variation of the NMO velocity and η (Vasconcelos and Tsvankin, 2006; Xu and Tsvankin, 2006). Here, we consider P-wave data from azimuthally anisotropic media with orthorhombic symmetry typical for fractured reservoirs (Schoenberg and Helbig, 1997; Bakulin et al., 2000; Grechka and Kachanov, 2006). Nonhyperbolic moveout of P-waves in

an orthorhombic layer with a horizontal symmetry plane is governed by the azimuths of the vertical symmetry planes, the symmetry-plane NMO velocities ($V_{\mathrm{nmo}}^{(1)}$ and $V_{\mathrm{nmo}}^{(2)}$) responsible for the NMO ellipse, and three anellipticity coefficients $\eta^{(1,2,3)}$ (Grechka and Tsvankin, 1999). Because the symmetry-plane NMO velocities and parameters $\eta^{(1,2,3)}$ depend on the fracture compliances and orientation (Bakulin et al., 2000), nonhyperbolic moveout inversion can help build physical models for reservoir characterization. Also, the parameters $V_{\mathrm{nmo}}^{(1,2)}$ and $\eta^{(1,2,3)}$ are sufficient to perform all P-wave time-processing steps in orthorhombic models (Grechka and Tsvankin, 1999).

For layered orthorhombic media, the parameters of the Alkhalifah-Tsvankin equation become effective quantities, and the interval values of $\eta^{(1,2,3)}$ can be estimated by a generalized Dix-type differentiation scheme based on the results of Vasconcelos and Tsvankin (2006) and Xu and Tsvankin (2006). However, this procedure is hampered by the same instability problems as the ones discussed above for the η inversion in layered VTI media.

Here, we propose to overcome the shortcomings of Dix-type techniques by employing the velocity-independent layer-stripping (VILS) method of Dewangan and Tsvankin (2006). This layer-stripping algorithm, which operates with reflection traveltimes, produces accurate interval long-spread reflection moveout, which can then be inverted for the layer parameters. We review the 2D version of VILS designed for VTI media and introduce a 3D implementation for wide-azimuth data from orthorhombic media. Numerical tests demonstrate that, in contrast to Dix-type inversion, our method remains robust in the presence of typical correlated noise in reflection traveltimes. Finally, we apply the algorithm to nonhyperbolic moveout analysis of wide-azimuth P-wave data acquired over a fractured reservoir at Rulison field in Colorado, U.S.A.

VELOCITY-INDEPENDENT LAYER STRIPPING

The velocity-independent layer-stripping algorithm of Dewangan and Tsvankin (2006) is based on the so-called PP + PS = SS method (Grechka and Tsvankin, 2002). VILS is entirely data driven and, if the model assumptions are satisfied, does not require knowledge of the velocity field anywhere in the medium.

2D layer stripping

Figure 1 shows 2D ray trajectories of pure-mode (non-converted) reflections from the top and bottom of the target zone overlain by a laterally homogeneous overburden. The incidence plane is supposed to represent a symmetry plane for the model as a whole, so that wave propagation is two-dimensional; this assumption becomes unnecessary in the 3D extension of the method discussed below. Although the target zone can be heterogeneous with interval curved interfaces, each layer in the overburden must be laterally homogeneous with a horizontal symmetry plane. Then the raypath of any reflection from the top of the target zone is symmetric with respect to the reflection point (e.g., points T or R in Figure 1).

As discussed by Dewangan and Tsvankin (2006), equalizing time slopes on common-receiver gathers at the source location $x^{(1)}$ can be used to identify the overburden reflection $x^{(1)}\mathrm{T}x^{(3)}$ that has the same horizontal slowness as the reflection $x^{(1)}\mathrm{TQR}x^{(2)}$ from the bottom of the target layer. This means that the reflections $x^{(1)}\mathrm{T}x^{(3)}$ and $x^{(1)}\mathrm{TQR}x^{(2)}$ share the downgoing leg $x^{(1)}\mathrm{T}$. Likewise, we can find the overburden reflection $x^{(2)}\mathrm{R}x^{(4)}$ that has the same upgoing leg $\mathrm{R}x^{(2)}$ as
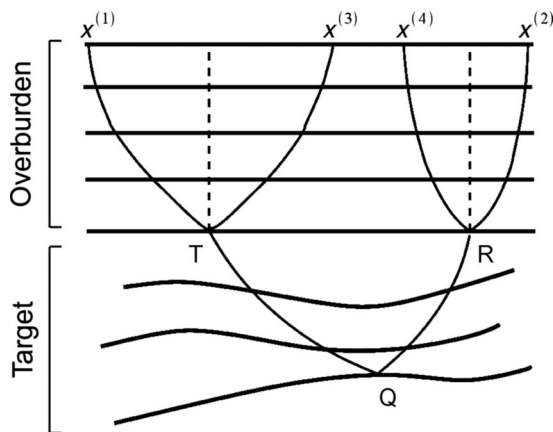

Figure 1. 2D diagram of the layer-stripping algorithm for pure-mode reflections (after Dewangan and Tsvankin, 2006). Points T and R are located at the bottom of the laterally homogeneous overburden. The leg $x^{(1)}\mathrm{T}$ is shared by the target reflection $x^{(1)}\mathrm{TQR}x^{(2)}$ and the overburden event $x^{(1)}\mathrm{T}x^{(3)}$; the leg $\mathrm{R}x^{(2)}$ is shared by the reflections $x^{(1)}\mathrm{TQR}x^{(2)}$ and $x^{(2)}\mathrm{R}x^{(4)}$.

the target event $x^{(1)} \mathbf{TQR} x^{(2)}$. Because any reflection path in the overburden is symmetric with respect to the reflection point, the interval reflection traveltime t^{int} in the target zone can be computed as

$$t^{\text{int}}(T,R) = t^{\text{eff}}(x^{(1)}, x^{(2)}) - \frac{1}{2}[t^{\text{ovr}}(x^{(1)}, x^{(3)}) + t^{\text{ovr}}(x^{(2)}, x^{(4)})], \tag{2}$$

where the superscripts "eff" and "ovr" refer to the target event $x^{(1)} \mathbf{TQR} x^{(2)}$ and the reflections from the bottom of the overburden, respectively. The corresponding source-receiver pair (T,R) has the following horizontal coordinates:

$$x_T = \frac{x^{(1)} + x^{(3)}}{2}, \quad x_R = \frac{x^{(2)} + x^{(4)}}{2}. \tag{3}$$

Equations 2 and 3 yield the interval reflection moveout function in the target zone without any information about the velocity model.

The 2D interval moveout-inversion methods based on ideas similar to those behind VILS have been developed by Van der Baan and Kendall (2002, 2003) and Fowler et al. (2008). In contrast to VILS, however, these methods assume the invariance of the horizontal slowness (ray parameter) along each ray, which implies that the target zone (not just the overburden) must be laterally homogeneous. Van der Baan and Kendall (2002, 2003) and Fowler et al. (2008) implement their algorithms for P-wave data from horizontally layered VTI media.

3D layer stripping for wide-azimuth data

The 3D version of the layer-stripping algorithm does not impose any restrictions on the properties (anisotropy, heterogeneity) of the target zone, but each layer in the overburden still must be laterally homogeneous with a horizontal symmetry plane. For wide-azimuth data (Figure 2), identifying the target and overburden reflections with the same ray segments requires estimating two orthogonal horizontal slowness components from reflection time slopes. In Figure 2, the horizontal slownesses of the target (eff) and overburden (ovr) reflections at location $\mathbf{x}^{(1)} = [x_1^{(1)}, x_2^{(1)}]$ can be obtained from

$$p_i^{\text{eff}}(\mathbf{x}^{(1)}, \mathbf{x}^{(2)}) = \left. \frac{\partial t^{\text{eff}}(\mathbf{x}, \mathbf{x}^{(2)})}{\partial x_i} \right|_{\mathbf{x} = \mathbf{x}^{(1)}}, \quad (i = 1,2) \tag{4}$$

and

$$p_i^{\text{ovr}}(\mathbf{x}^{(1)}, \mathbf{x}^{(3)}) = \left. \frac{\partial t^{\text{ovr}}(\mathbf{x}, \mathbf{x}^{(3)})}{\partial x_i} \right|_{\mathbf{x} = \mathbf{x}^{(1)}}, \quad (i = 1,2). \tag{5}$$

Using equations 4 and 5, we find the location $\mathbf{x}^{(3)}$, for which the time slopes (horizontal slownesses) of the two events are identical:

$$p_i^{\text{eff}}(\mathbf{x}^{(1)}, \mathbf{x}^{(2)}) = p_i^{\text{ovr}}(\mathbf{x}^{(1)}, \mathbf{x}^{(3)}), \quad (i = 1,2). \tag{6}$$

Therefore, the reflections $\mathbf{x}^{(1)} \mathbf{TQR} \mathbf{x}^{(2)}$ and $\mathbf{x}^{(1)} \mathbf{T} \mathbf{x}^{(3)}$ have the common leg $\mathbf{x}^{(1)} \mathbf{T}$. The same operation applied at point $\mathbf{x}^{(2)}$ helps to find the overburden reflection $\mathbf{x}^{(2)} \mathbf{R} \mathbf{x}^{(4)}$ that shares the upgoing leg $\mathbf{R} \mathbf{x}^{(2)}$ with the target event $\mathbf{x}^{(1)} \mathbf{TQR} \mathbf{x}^{(2)}$. The interval reflection traveltime can then be obtained from equation 2. Because $\mathbf{T}$ and $\mathbf{R}$ represent the

midpoints of the corresponding source-receiver pairs, their horizontal coordinates can be easily found from $\mathbf{x}^{(1)}, \mathbf{x}^{(2)}, \mathbf{x}^{(3)}$, and $\mathbf{x}^{(4)}$.

Thus, the velocity-independent layer-stripping algorithm makes it possible to construct interval moveout functions in two and three dimensions. Because reflection traveltimes can be estimated with relatively high accuracy, VILS helps to avoid the stability problems in Dix-type inversion caused by trade-offs between the effective moveout parameters.

Similar to the original version of the PP + PS = SS method, our layer-stripping algorithm operates with reflection traveltimes. Grechka and Dewangan (2003) develop an efficient implementation of the PP + PS = SS method by replacing traveltime analysis with a convolution of recorded PP and PS traces. Their technique can be adapted to compute interval P-wave reflection data using reflections from the top and bottom of the target layer. Although the convolution of recorded traces cannot produce the correct amplitudes, the constructed arrivals should have the kinematics of P-wave primary reflections and, therefore, are suitable for interval moveout analysis.

TESTS ON SYNTHETIC DATA

Next, we test the layer-stripping algorithm on 2D and 3D longspread P-wave data generated by kinematic ray tracing (Gajewski and Pšenčík, 1987) for VTI and orthorhombic models. Reflected arrivals on the synthetic seismograms are obtained by placing the Ricker wavelet at the corresponding reflection traveltime. The interval moveout parameters in the target layer are estimated from our method and the Dix-type equations. To compare the stability of the two techniques in the presence of correlated noise, we add several noise functions to the input traveltimes.

2D inversion for VTI media

For stratified VTI media composed of N horizontal layers, longspread P-wave traveltime is described by equation 1 with effective moveout parameters (Grechka and Tsvankin, 1998; Tsvankin, 2005):
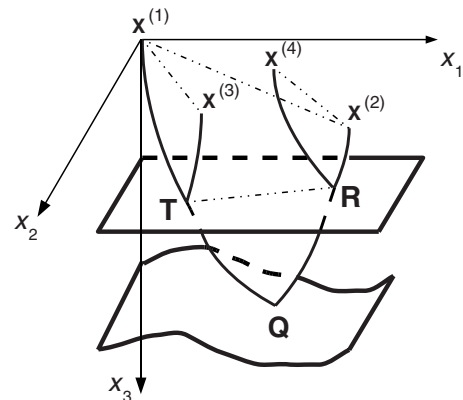

Figure 2. 3D diagram of the layer-stripping algorithm. Points $\mathbf{T}$ and $\mathbf{R}$ are located at the bottom of the laterally homogeneous overburden. The sources and receivers ($\mathbf{x}^{(1)}, \mathbf{x}^{(2)}, \mathbf{x}^{(3)}$, and $\mathbf{x}^{(4)}$) are placed at the surface but not necessarily along a straight line. The reflection point $\mathbf{Q}$ is located at the bottom of the target layer, which can be arbitrarily anisotropic and heterogeneous. The leg $\mathbf{x}^{(1)} \mathbf{T}$ is shared by the target event $\mathbf{x}^{(1)} \mathbf{TQR} \mathbf{x}^{(2)}$ and the overburden reflection $\mathbf{x}^{(1)} \mathbf{T} \mathbf{x}^{(3)}$; the leg $\mathbf{R} \mathbf{x}^{(2)}$ is shared by the reflections $\mathbf{x}^{(1)} \mathbf{TQR} \mathbf{x}^{(2)}$ and $\mathbf{x}^{(2)} \mathbf{R} \mathbf{x}^{(4)}$.

$$t^2(N) = t_0^2(N) + \frac{x^2}{V_{\text{nmo}}^2(N)}$$
$$- \frac{2\,\eta(N)\,x^4}{V_{\text{nmo}}^2(N)\{t_0^2(N)V_{\text{nmo}}^2(N) + [1 + 2\,\eta(N)]x^2\}}. \tag{7}$$

The effective NMO velocity is found from the Dix equation,

$$V_{\text{nmo}}^2(N) = \frac{1}{t_0(N)} \sum_{i=1}^{N} (V_{\text{nmo}}^{(i)})^2 t_0^{(i)}, \tag{8}$$

where $t_0^{(i)}$ and $V_{\text{nmo}}^{(i)}$ are the interval values in layer i. The effective parameter η is approximately given by

$$\eta(N) = \frac{1}{8} \left\{ \frac{1}{V_{\text{nmo}}^4(N)\,t_0(N)} \left[\sum_{i=1}^{N} (V_{\text{nmo}}^{(i)})^4 (1 + 8\,\eta^{(i)})\, t_0^{(i)} \right] \right.$$
$$\left. - 1 \right\}. \tag{9}$$

The best-fit effective parameters V_{nmo} and η for the top and bottom of a layer of interest usually are obtained by applying semblance-based nonhyperbolic moveout inversion to long-spread P-wave data. Then the interval V_{nmo} can be computed from equation 8:

Table 1. Interval parameters of a three-layer VTI model (model 1).

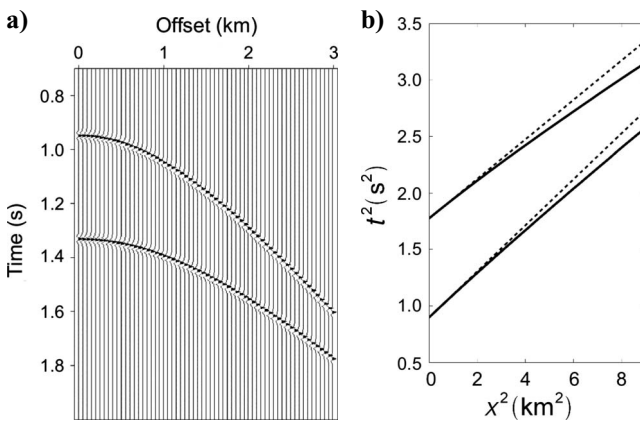| Layer	Thickness (km)	t_0 (s)	V_{nmo} (km/s)	η
1	0.7	0.70	2.10	0
2	0.3	0.25	2.52	0.10
3[a]	0.5	0.39	2.78	0.20

[a] Target layer

Figure 3. (a) Synthetic long-spread reflections from the top and bottom of layer 3 (target) in model 1. (b) The $t^2(x^2)$ function (solid lines) for both events shown in plot (a). The dashed lines mark the hyperbolic moveout function, $t^2 = t_0^2 + (x^2/V_{\text{nmo}}^2)$. The model parameters are listed in Table 1.

$$(V_{\text{nmo}}^{(i)})^2 = \frac{V_{\text{nmo}}^2(i)\,t_0(i) - V_{\text{nmo}}^2(i-1)\,t_0(i-1)}{t_0(i) - t_0(i-1)}. \tag{10}$$

Equation 9 yields the interval η:

$$\eta^{(i)} = \frac{1}{8(V_{\text{nmo}}^{(i)})^4} \left[\frac{g(i)t_0(i) - g(i-1)t_0(i-1)}{t_0(i) - t_0(i-1)} - (V_{\text{nmo}}^{(i)})^4 \right]; \tag{11}$$

$$g(N) \equiv V_{\text{nmo}}^4(N)[1 + 8\,\eta(N)].$$

Although equations 1 and 7 provide a good approximation for nonhyperbolic moveout in VTI media, the estimated η is sensitive to small errors in V_{nmo} even if the maximum offset-to-depth ratio (x_{max}/D) is between two and three. The trade-off between the effective V_{nmo} and η (along with the slight bias of the nonhyperbolic moveout equation) causes substantial instability in the η estimation, which is amplified in the Dix-type layer stripping based on equation 11 (Grechka and Tsvankin, 1998).

Model 1

The first numerical test was performed for the three-layer VTI model with the parameters listed in Table 1 (Figure 3a; $x_{\text{max}}/D = 2$ for the bottom of the model). Both VILS and the Dix-type method were used to estimate the interval parameters V_{nmo} and η in the third layer. Although the η values in this model are moderate, the traveltime curves for the top and bottom of the target layer noticeably deviate from the hyperbolic moveout approximation at large offsets (Figure 3b).

To reconstruct the reflection traveltimes from the top and bottom of the target (third) layer, we used 2D semblance search for V_{nmo} and η based on equation 7. (Note that equations 1 and 7 are equivalent in terms of semblance analysis.) Then VILS was applied to compute the interval traveltimes, which were inverted for the interval parameters using least-squares fitting of moveout equation 1 (see the flow chart in Figure 4). The interval value of η estimated by VILS is quite accurate, with the error (just 0.02) caused mostly by the slight bias of equation 1 discussed by Grechka and Tsvankin (1998).

The semblance analysis for the top and bottom of the target layer also provides input data for the Dix-type differentiation described above. However, in contrast to VILS, the Dix-type algorithm operates with the effective moveout parameters, not traveltimes. As a result, small distortions in the effective η estimates are amplified in the layer-stripping procedure, which leads to an error of 0.06 in the interval η value.

Error analysis

To study the influence of realistic noise on interval parameter estimation, we added random, linear, and sinusoidal time errors to the reflection moveout from the bottom of the target layer. The traveltimes from the top of the target were left unchanged. As before, the input data for VILS and the Dix-type method were obtained from a 2D semblance search based on equation 7.

Both methods use semblance analysis, so they remain reasonably stable in the presence of random noise. For random errors with the magnitude approaching 10 ms (Figure 5), the interval η estimated by VILS is distorted by less than 0.02, while the Dix-type method produces η errors in the range of 0.05–0.08.

The second type of noise used in our tests is linear, which can simulate long-period statics errors. For a relatively large error that changes from 6 ms at zero offset to -6 ms at the maximum offset, VILS estimates the interval V_{nmo} and η with errors of 4% and 0.07, respectively. The distortions in V_{nmo} and η after the Dix-type layer stripping are much larger (15% and 0.34, respectively), which makes the inversion practically useless. These results are consistent with the analysis in Grechka and Tsvankin (1998), who demonstrate that linear time noise of a somewhat smaller magnitude may cause errors in the effective η close to 0.1. The Dix-type procedure increases such errors by a factor that depends on the relative thickness of the target layer (i.e., on the ratio of its thickness and depth).

Next, we contaminated the data with a sinusoidal time function designed to emulate short-period statics errors: $t = A \sin(n\pi x/x_{max})$. The interval parameter-estimation results for different values of A and n are listed in Table 2. The error in the interval η produced by VILS reaches only 0.08 even for $A = 8$ ms, whereas the Dix-type method breaks down for $A \gtrsim 3$ ms.

These tests clearly demonstrate the superior stability of VILS in the presence of typical correlated noise in reflection traveltimes. Even relatively small time errors can cause substantial distortions in the effective moveout parameters, which propagate with amplification into the interval η values. In contrast, percentage errors in the traveltimes themselves are insignificant, which ensures the high accuracy of the interval moveout produced by VILS.

Influence of lateral heterogeneity

The layer-stripping procedure in VILS is based on the assumption that each layer in the overburden is laterally homogeneous and has a horizontal symmetry plane. Lateral velocity gradients or dipping interfaces make the raypaths of overburden events asymmetric with respect to the reflection point, which may cause errors in equations 2 and 3. Note that lateral heterogeneity above the reflector also violates the assumptions behind the Dix-type method (Alkhalifah and Tsvankin, 1995; Grechka and Tsvankin, 1998).

To evaluate the influence of mild dips in the overburden on interval parameter estimation, we tilted the most shallow reflector in model 1 by 10° (Figure 6). Then we generated noise-free synthetic data and applied VILS and the Dix-type method without taking the dip into account. The interval parameters V_{nmo} and η in the third layer estimated by VILS are distorted by only 2% and 0.05, respectively. In contrast, the Dix-type method produces more significant errors in the interval values, reaching 6% in V_{nmo} and 0.15 in η. This and other tests indicate that VILS is much less sensitive to mild lateral heterogeneity than the Dix differentiation.

3D inversion for orthorhombic media

The azimuthally dependent P-wave reflection moveout in a horizontal orthorhombic layer can be well approximated by equation 1 with azimuthally varying parameters V_{nmo} and η (Xu and Tsvankin, 2006; Vasconcelos and Tsvankin, 2006):

$$t^2(x,\alpha) = t_0^2 + \frac{x^2}{V_{nmo}^2(\alpha)}$$
$$- \frac{2\eta(\alpha)x^4}{V_{nmo}^2(\alpha)[t_0^2 V_{nmo}^2(\alpha) + (1 + 2\eta(\alpha))x^2]},$$
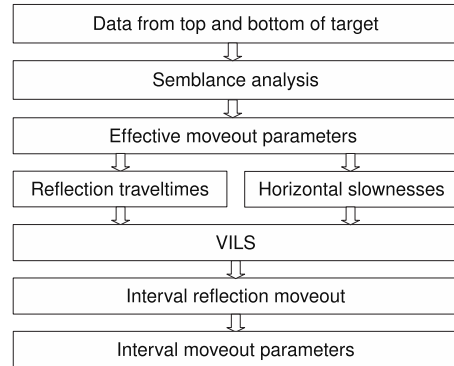
(12)

Figure 4. Workflow for interval parameter estimation using VILS.
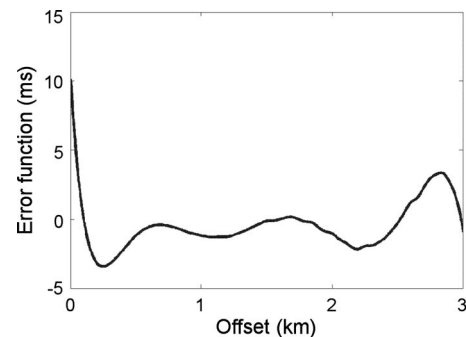

Figure 5. Random traveltime error with the maximum magnitude close to 10 ms.

Table 2. Influence of correlated noise on the interval parameter estimation for the third layer in model 1. A sinusoidal error function ($t = A \sin(n\pi x/x_{max})$) was added to the traveltimes from the bottom of the layer. The table shows the percentage error in the interval velocity V_{nmo} and the absolute error in the interval η estimated by VILS and the Dix-type method for different combinations of A and n.

Parameters of error function	$A = 3$ ms, $n = 3$		$A = 3$ ms, $n = 2$		$A = 8$ ms, $n = 3$	
Inversion error	V_{nmo} (%)	η	V_{nmo} (%)	η	V_{nmo} (%)	η
VILS	0.6	0.01	0.0	0.00	2.1	0.08
Dix	11	0.19	8.2	0.13	21	0.41

where α is the source-to-receiver azimuth. The azimuthally dependent NMO velocity is obtained from the equation of the NMO ellipse:

$$V_{nmo}^{-2}(\alpha) = \frac{\sin^2(\alpha - \varphi)}{[V_{nmo}^{(1)}]^2} + \frac{\cos^2(\alpha - \varphi)}{[V_{nmo}^{(2)}]^2}; \qquad (13)$$

φ is the azimuth of the $[x_1, x_3]$ symmetry plane, and $V_{nmo}^{(1)}$ and $V_{nmo}^{(2)}$ are the NMO velocities in the vertical symmetry planes $[x_2, x_3]$ and $[x_1, x_3]$, respectively. The parameter η is approximately given by (Pech and Tsvankin, 2004)

$$\eta(\alpha) = \eta^{(1)} \sin^2(\alpha - \varphi) + \eta^{(2)} \cos^2(\alpha - \varphi)$$
$$- \eta^{(3)} \sin^2(\alpha - \varphi) \cos^2(\alpha - \varphi), \qquad (14)$$

where $\eta^{(1)}$, $\eta^{(2)}$, and $\eta^{(3)}$ are the anellipticity coefficients defined in the $[x_2, x_3], [x_1, x_3]$, and $[x_1, x_2]$ symmetry planes, respectively.

For layered orthorhombic media, all moveout parameters become effective quantities. The semiaxes and orientation of the effective NMO ellipse (equation 13) can be obtained from the generalized Dix equation by averaging the interval NMO ellipses (Grechka et al., 1999). If the vertical symmetry planes in different layers are misaligned, the principal directions for the effective parameter η are described by a separate azimuth φ_1 (Xu and Tsvankin, 2006):

$$\eta(\alpha) = \eta^{(1)} \sin^2(\alpha - \varphi_1) + \eta^{(2)} \cos^2(\alpha - \varphi_1)$$
$$- \eta^{(3)} \sin^2(\alpha - \varphi_1) \cos^2(\alpha - \varphi_1). \qquad (15)$$
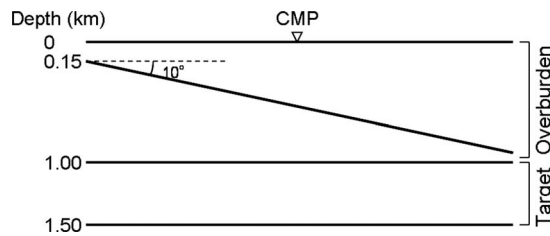

Figure 6. Three-layer VTI model used to evaluate the influence of mild dip (10°) in the overburden on the inversion results. Except for the dip, all medium parameters are the same as those in model 1 (Table 1). The lateral extent of the model is 4 km; the common midpoint (CMP) used for parameter estimation is located in the middle.

The effective parameter η for each azimuth α can be computed from the VTI equation 9 because kinematic signatures in each vertical plane of layered orthorhombic media can be approximately described by the corresponding VTI equations (Tsvankin, 1997, 2005). Then the parameters $\eta^{(1)}$, $\eta^{(2)}$, $\eta^{(3)}$, and φ_1 can be found by fitting equation 15 to the effective η values for a wide range of azimuths.

To implement VILS and the Dix-type inversion for layered orthorhombic media, we use the 3D nonhyperbolic semblance algorithm of Vasconcelos and Tsvankin (2006) based on equations 12, 13, and 15. The best-fit effective moveout parameters $V_{nmo}^{(1,2)}$, $\eta^{(1,2,3)}$, φ, and φ_1 for the top and bottom of the target layer are found by a multidimensional semblance search using the full range of available offsets and azimuths. For purposes of the Dix-type layer stripping, the interval NMO ellipse is obtained from the generalized Dix equation (Grechka et al., 1999) and the interval η value for each azimuth is computed from the VTI equation 11. Finally, the interval parameters $\eta^{(1,2,3)}$ are estimated by fitting equation 14 to the azimuthally varying η values.

The long-spread, wide-azimuth reflection traveltimes produced by the nonhyperbolic semblance analysis also serve as the input data for VILS (see the flow chart in Figure 4). To apply VILS to 3D wide-azimuth data (Figure 2), it is also necessary to estimate the horizontal slowness components at the source and receiver locations. In principle, the horizontal projections of the slowness vector (equations 4 and 5) can be computed from reflection traveltimes on common-shot or common-receiver gathers. A more stable and efficient option, however, is to express the horizontal slownesses as functions of offset and azimuth through the best-fit moveout parameters using equation 12. Despite the parameter trade-offs, equation 12 provides sufficient accuracy for long-spread P-wave moveout and, therefore, for the traveltime derivatives. After the interval traveltimes are computed by VILS, the interval parameters φ, $V_{nmo}^{(1,2)}$, and $\eta^{(1,2,3)}$ are obtained by least-squares fitting of equation 12 to the estimated traveltimes for a wide range of offsets and azimuths.

Model 2

The 3D parameter-estimation algorithm was first tested on an orthorhombic layer overlain by VTI and isotropic layers (Table 3). VILS and the Dix-type method were applied to long-spread ($x_{max}/D = 2$ for the bottom of the model), wide-azimuth data from the top and bottom of the orthorhombic layer. The model is laterally homogeneous, so synthetic data were generated for a single source location and a full (180°) range of source-receiver azimuths. To ensure the stability of 3D nonhyperbolic moveout inversion, the receivers were placed on 19 lines with an azimuthal interval of 10°. As illustrated by Figure 7, the azimuthal anisotropy in the target layer

Table 3. Interval parameters of a three-layer model used to test the 3D layer-stripping algorithm (model 2).

Layer	Symmetry type	Thickness (km)	t_0 (s)	$V_{nmo}^{(1)}$ (km/s)	$V_{nmo}^{(2)}$ (km/s)	$\eta^{(1)}$	$\eta^{(2)}$	$\eta^{(3)}$	φ (°)
1	ISO	0.5	0.50	2.0	2.0	0	0	0	—
2	VTI	0.5	0.41	2.49	2.49	0.05	0.05	0	—
3[a]	ORTH	0.5	0.39	3.18	2.64	0.2	0.06	0.13	30

[a] Target layer
ISO — Isotropic
ORTH — Orthorhombic

makes the traveltimes from its bottom vary with azimuth. Without traveltime noise, both methods give similar accuracy in the interval moveout parameters.

Error analysis

As before, we added linear and sinusoidal time errors to the reflection moveout from the bottom of the target layer in model 2. For the azimuthally invariant linear error that changes from 6 ms at zero offset to -6 ms at the maximum offset, the interval parameters $V_{nmo}^{(1,2)}$ and $\eta^{(1,2,3)}$ estimated by VILS are distorted by no more than 3% and 0.06, respectively. The Dix-type method produces much larger errors, reaching 9% in $V_{nmo}^{(1,2)}$ and 0.16 in $\eta^{(1,2,3)}$. The errors in the symmetry-plane azimuth φ for both methods are negligible.

We also contaminated the traveltimes with the noise function of the form $t(x,\alpha) = A \sin(n\pi x/x_{max})\sin m\alpha$ (Table 4). The coefficients n and m control the period of the error in the radial and azimuthal directions, respectively. In general, inversion errors tend to be higher when m is an even number. If the error function does not vary with azimuth ($m = 0$), both methods give more accurate results for even values of n, which agrees with the conclusions of Xu and Tsvankin (2006). As illustrated by several examples in Table 4, even for noisy data with $A = 10$ ms, VILS produces errors in the interval $\eta^{(1,2,3)}$ not exceeding 0.09. The Dix-type method distorts the η parameters by up to 0.22 and the NMO velocities by 10%.

It is interesting that despite the complexity of orthorhombic symmetry, the Dix-type method gives much better results for model 2 than for the VTI model 1 (compare Tables 2 and 4). Most likely, this improvement is explained by wide azimuthal coverage in 3D inversion, which creates redundancy and makes the estimation of the effective moveout parameters more stable.

Next, we studied the influence of the thickness of the target layer in model 2 on the inversion results. Any layer-stripping method inevitably becomes less accurate as the layer of interest becomes thinner. We added the sinusoidal error with $A = 3$ ms, $n = 3$, and $m = 0$ to the traveltimes from the bottom of the target and reduced its thickness until it reached 0.15 km (Table 5). VILS gives acceptable results for the interval V_{nmo} and η when the thickness exceeds 0.25 km (i.e., when the thickness-to-depth ratio exceeds 0.2), whereas the error in V_{nmo} estimated by the Dix-type method approaches 10%. However, VILS breaks down for the target layer that is only 0.15 km thick.

Model 3

The third model includes the target orthorhombic layer beneath the overburden composed of isotropic and orthorhombic layers (Table 6). Note that the vertical symmetry planes in the two orthorhombic layers are misaligned, so the azimuthally varying parameter η from the bottom of the target is described by equation 15. The vertical variation of the symmetry-plane azimuths does not cause any complications in the application of VILS, as long as the overburden is laterally homogeneous and has a horizontal symmetry plane.

The accuracy of VILS and the Dix-type method for noise-free data is similar, which was also the case for model 2. The sinusoidal error

$t = A \sin(n\pi x/x_{max})$ applied to the traveltimes from the bottom of the target layer produces much more significant distortions in the output of the Dix-type differentiation compared to VILS. For instance, when $A = 6$ ms and $n = 3$, the maximum errors in the interval $V_{nmo}^{(1,2)}$ and $\eta^{(1,2,3)}$ estimated by VILS are 4% and 0.09 (respectively), wheras the corresponding errors of the Dix-type method reach 13% and 0.25.

FIELD-DATA EXAMPLE

The 3D VILS algorithm was applied to wide-azimuth P-wave data acquired by the Reservoir Characterization Project (RCP, a research consortium at Colorado School of Mines) at Rulison field, a basin-centered gas accumulation in South Piceance Basin, Colorado. The reservoir (Williams Fork Formation) is capped by the Upper Mesaverde (UMV) Shale, which served as the target layer in our study (Figure 8).

Xu and Tsvankin (2007) apply a comprehensive anisotropic processing sequence to the data and analyze the effective and interval NMO ellipses as well as the azimuthal AVO response. We used the same data set, which was acquired in 2003 and preprocessed for azi-
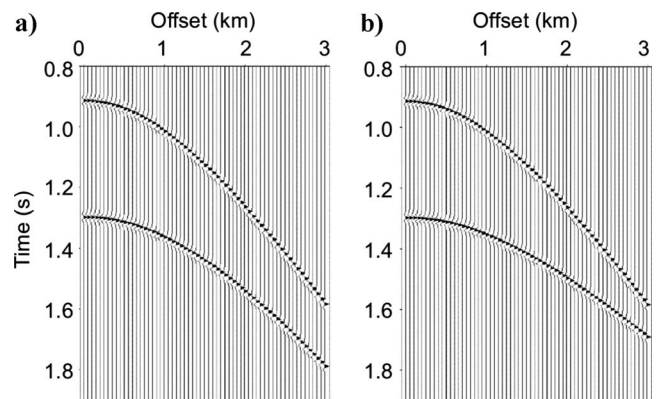

Figure 7. Synthetic long-spread P-wave reflections from the top and bottom of layer 3 (target) in model 2 (Table 3). The seismograms are computed in the two orthogonal vertical symmetry planes of the target orthorhombic layer; (a) $\alpha = 30°$, (b) $\alpha = 120°$.

Table 4. Influence of correlated noise on the interval parameter estimation for the third layer in model 2. A sinusoidal error function ($A \sin(n\pi x/x_{max})\sin m\alpha$) was added to the traveltimes from the bottom of the layer. The table shows the maximum percentage error in the interval velocities $V_{nmo}^{(1,2)}$ and the maximum absolute error in the interval $\eta^{(1,2,3)}$ estimated by VILS and the Dix-type method. The errors in the azimuth φ do not exceed 0.5° for both methods.

	$A = 3$ ms		$A = 3$ ms		$A = 10$ ms	
Parameters of error function	$n = 3, m = 0$		$n = 3, m = 2$		$n = 3, m = 0$	
Inversion error	V_{nmo} (%)	η	V_{nmo} (%)	η	V_{nmo} (%)	η
VILS	1.2	0.04	1.0	0.02	2.4	0.09
Dix	4.4	0.09	2.3	0.08	10	0.22

muthal moveout and AVO analysis. Because the subsurface structure is close to horizontally layered (Figure 9), the moveout equations discussed above should give an accurate description of reflection traveltimes. As suggested by Xu and Tsvankin (2007), we combined CMP gathers into 5×5 superbins to increase the azimuthal and offset coverage. The moveout inversion was carried out in the center of the RCP survey area (Figure 10), where the coverage is sufficient for minimizing the influence of the acquisition footprint.

Because the maximum offset-to-depth ratio at the bottom of the reservoir is close to unity (on average for the study area), nonhyperbolic moveout inversion cannot be applied to the reservoir formation. Therefore, we performed parameter estimation for the UMV Shale, the layer between the Mesaverde Top and the top of the reservoir (Figure 8). In the center of the study area, the offset-to-depth ratio at the bottom of the shale is between 1.9 and 2.2. To estimate the interval moveout parameters, we used the VILS and Dix-type algorithms for layered orthorhombic media discussed above.

Our tests show that the NMO ellipticity is small for the top and bottom of the target shale layer over most of the area. Therefore, the principal directions of the effective and interval NMO ellipses are poorly constrained by the data. However, as long as the offset-to-depth ratio is close to two, the parameters $\eta^{(1,2,3)}$ can be estimated reliably. The interval values of $\eta^{(1,2,3)}$ for two superbin gathers near the center of the area are listed in Table 7.

Although there is no independent information about the actual anellipticity parameters in the field, the values produced by VILS are much more plausible than those computed from the Dix-type equations. First, the Dix-derived interval parameters $\eta^{(1,2,3)}$ are too large

for shale formations and lie outside the range suggested by laboratory and field studies (Wang, 2002; Tsvankin, 2005). The interval value of $\eta^{(2)}$ for the first superbin even exceeds unity. Also, horizontal shale layers typically exhibit weak (if any) azimuthal anisotropy unless they are fractured. Available geologic information for Rulison field and the small eccentricity of the NMO ellipses suggest that the symmetry of the UMV Shale over most of the study area is close to VTI. This implies that the difference between the parameters $\eta^{(1)}$ and $\eta^{(2)}$, as well as the magnitude of $\eta^{(3)}$, should be relatively small, which agrees with the output of VILS. The values of $\eta^{(2)}$ for both superbins produced by the Dix-type method, however, are much larger than those of $\eta^{(1)}$.

To test the stability of both methods, we also added a linear time error (from 4 ms at zero offset to -4 ms at the maximum offset for each azimuth) to the reflection moveout from the bottom of the shale layer in the second superbin. The interval parameters $\eta^{(1,2,3)}$ estimated by VILS change only by -0.06, -0.07, and 0.01, respectively, while the corresponding variations produced by the Dix-type method are much larger (-0.12, -0.21, and 0.13). Hence, VILS is more stable than the Dix-type method in the presence of correlated time errors, as established above for the synthetic data.

The NMO ellipticity in the UMV Shale is pronounced only near the east boundary of the study area (Xu and Tsvankin, 2007). Because of the small offset-to-depth ratio (between 1 and 1.3) for the bottom of the shale layer near the area boundary, the inverted parameters $\eta^{(1,2,3)}$ are unstable and are likely to contain large errors. The interval velocities $V_{\mathrm{nmo}}^{(1,2)}$ and the azimuth φ estimated by both methods for two adjacent superbin gathers in the area of substantial NMO ellipticity are listed in Table 8. As before, we added a linear time error (from 2 ms at zero offset to -2 ms at the maximum offset for each azimuth) to the traveltimes from the bottom of the shale in the second superbin, which causes a deviation of about 3% in the effective velocities $V_{\mathrm{nmo}}^{(1,2)}$. As a result, the interval parameters $V_{\mathrm{nmo}}^{(1,2)}$ and φ estimated by the Dix-type method change by 13%, 16%, and 4°, respectively. The sensitivity of VILS to the time error is much lower, with the NMO velocities changing by less than 8% and φ by 1°. Despite the superior performance by VILS, the errors in $V_{\mathrm{nmo}}^{(1,2)}$ are relatively large, primarily because of the small thickness of the target layer (the thickness-to-depth ratio is about 0.2). Still, this result shows that it may be beneficial to apply VILS to interval NMO-velocity estimation from conventional-spread data.

Table 5. Errors of the interval $V_{\mathrm{nmo}}^{(1,2)}$ and $\eta^{(1,2,3)}$ for two different thicknesses of the target layer in model 2 (Table 3). The traveltimes from the bottom of the target are contaminated by the sinusoidal noise function with $A = 3$ ms, $n = 3$, and $m = 0$.

Thickness (km)	0.35		0.15	
Inversion error	V_{nmo} (%)	η	V_{nmo} (%)	η
VILS	2.2	0.05	8.3	0.15
Dix	7.5	0.13	20	0.38

Table 6. Interval parameters of a three-layer model that includes two orthorhombic layers with misaligned vertical symmetry planes (model 3).

Layer	Symmetry type	Thickness (km)	t_0 (s)	$V_{\mathrm{nmo}}^{(1)}$ (km/s)	$V_{\mathrm{nmo}}^{(2)}$ (km/s)	$\eta^{(1)}$	$\eta^{(2)}$	$\eta^{(3)}$	φ (°)
1	ISO	0.3	0.30	2	2	0	0	0	—
2	ORTH	0.7	0.58	2.56	3.06	0.05	0.07	0.02	30
3[a]	ORTH	0.5	0.39	3.68	2.73	0.24	0.12	-0.10	70

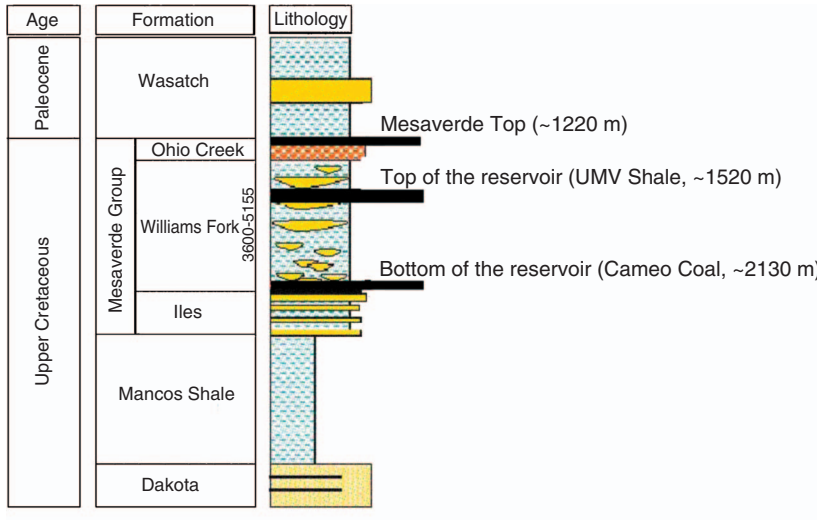[a] Target layer
ISO — Isotropic
ORTH — Orthorhombic

Figure 8. Stratigraphic column of Rulison field (after Xu and Tsvankin, 2007). The gas-producing reservoir is bounded by the UMV Shale (the target layer in this study) and the Cameo Coal.
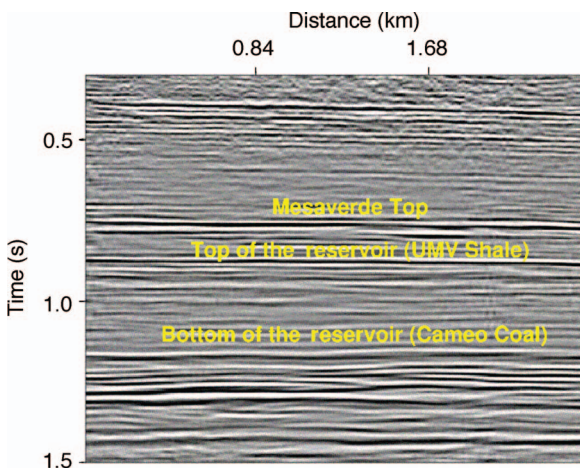

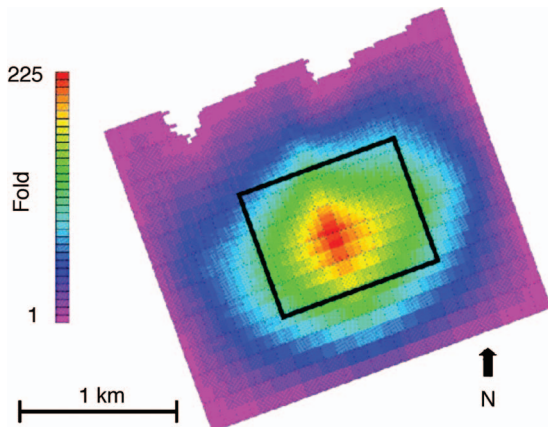Figure 9. Seismic section across the middle of the survey area at Rulison field (after Xu and Tsvankin, 2007).

Figure 10. P-wave fold for the 16.8×16.8 m bin size at Rulison field (after Xu and Tsvankin, 2007). The rectangle in the center marks the study area of our paper.

Table 7. Interval parameters $\eta^{(1,2,3)}$ estimated for two superbin gathers in the center of the study area at Rulison field.

Superbin	1			2		
	$\eta^{(1)}$	$\eta^{(2)}$	$\eta^{(3)}$	$\eta^{(1)}$	$\eta^{(2)}$	$\eta^{(3)}$
VILS	0.38	0.47	−0.18	0.24	0.31	−0.15
Dix	0.74	1.24	−0.35	0.31	0.62	−0.19

Table 8. Interval NMO ellipses for two superbin gathers near the east boundary of the study area.

Superbin	1			2		
	$V_{nmo}^{(1)}$ (km/s)	$V_{nmo}^{(2)}$ (km/s)	φ (°)	$V_{nmo}^{(1)}$ (km/s)	$V_{nmo}^{(2)}$ (km/s)	φ (°)
VILS	4.22	3.99	115	4.33	3.84	122
Dix	4.26	3.82	104	4.41	3.91	139

CONCLUSIONS

We combined velocity-independent layer stripping with nonhyperbolic moveout inversion to estimate the interval parameters of VTI and orthorhombic media. Whereas Dix-type differentiation algorithms operate with effective moveout parameters, VILS is based on layer stripping of reflection traveltimes. If the overburden is laterally homogeneous and has a horizontal symmetry plane, VILS produces exact interval traveltimes without any information about the velocity field. Then the interval traveltime function is inverted for the relevant parameters of the target layer using moveout equations for a homogeneous medium.

Because effective traveltimes are much better constrained by reflection data than effective moveout parameters, VILS gives more stable interval parameter estimates than Dix-type techniques. In particular, our synthetic tests on noise-contaminated data confirm that VILS can substantially increase the accuracy of nonhyperbolic moveout inversion for the interval time-processing parameter η in VTI media. The addition of small linear or sinusoidal time errors causes pronounced distortions in the effective η values, which are further enhanced by Dix-type layer stripping. In contrast, the interval moveout function produced by VILS is weakly sensitive to moderate levels of noise in the input traveltimes, ensuring a higher stability of the interval η estimates. Our tests show that VILS remains sufficiently accurate for VTI media in the presence of mild lateral heterogeneity (e.g., dips of up to 10°) in the overburden.

We also discussed an extension of VILS to 3D wide-azimuth P-wave data from azimuthally anisotropic models composed of orthorhombic and TI layers. To identify the target and overburden reflections that share the same ray segments, we obtain the horizontal slowness components from the best-fit effective moveout parameters, which helps avoid direct differentiation of traveltimes and reduces the computational cost. Then the interval moveout produced by VILS is inverted for the azimuths of the vertical symmetry planes, symmetry-direction NMO velocities, and anellipticity parameters $\eta^{(1,2,3)}$. Wide azimuthal coverage helps increase the stability of η estimation using 3D Dix-type layer stripping. Nevertheless, numerical testing clearly demonstrates the higher accuracy of VILS for typical orthorhombic models, including those with the depth-varying azimuths of the vertical symmetry planes.

The 3D version of the method was successfully tested on wide-azimuth P-wave reflections from an anisotropic shale layer at Rulison field in Colorado. For long-spread superbin gathers in the center of the study area, VILS yields more plausible and stable values of the interval parameters $\eta^{(1,2,3)}$ than the Dix-type method. Near the eastern boundary of the study area, where the offset-to-depth ratio is smaller and the η parameters are poorly constrained, application of VILS helps obtain a better estimate of the interval NMO ellipse.

It should be mentioned that the superior accuracy of VILS is achieved at the expense of its somewhat higher (compared to the Dix-type algorithms) computational cost. In addition to matching reflection time slopes at the surface, it is necessary to carry out nonhyperbolic moveout inversion not only for recorded reflection events but also for the interval moveout function. However, our implementation of VILS for horizontally layered media is much more efficient than the general version of the method because time slopes are calculated directly from the moveout parameters.

REFERENCES

Alkhalifah, T., 1997, Velocity analysis using nonhyperbolic moveout in transversely isotropic media: Geophysics, **62**, 1839–1854.
Alkhalifah, T., and I. Tsvankin, 1995, Velocity analysis for transversely isotropic media: Geophysics, **60**, 1550–1566.
Bakulin, A., V. Grechka, and I. Tsvankin, 2000, Estimation of fracture parameters from reflection seismic data, Part II: Fractured models with orthorhombic symmetry: Geophysics, **65**, 1803–1817.
Dewangan, P., and I. Tsvankin, 2006, Velocity-independent layer stripping of PP and PS reflection traveltimes: Geophysics, **71**, no. 4, U59–U65.
Dix, C. H., 1955, Seismic velocities from surface measurements: Geophysics, **20**, 68–86.
Fowler, P. J., A. Jackson, J. Gaffney, and D. Boreham, 2008, Direct nonlinear traveltime inversion in layered VTI media: 78th Annual International

Meeting, SEG, Expanded Abstracts, 3028–3032.

Gajewski, D., and I. Pšenčík, 1987, Computation of high frequency seismic wavefields in 3-D laterally inhomogeneous anisotropic media: Geophysical Journal of the Royal Astronomical Society, **91**, 383–412.

Grechka, V., and P. Dewangan, 2003, Generation and processing of pseudo-shear-wave data: Theory and case study: Geophysics, **68**, 1807–1816.

Grechka, V., and M. Kachanov, 2006, Seismic characterization of multiple fracture sets: Does orthotropy suffice?: Geophysics, **71**, no. 3, D93–D105.

Grechka, V., A. Pech, and I. Tsvankin, 2002, Multicomponent stacking-velocity tomography for transversely isotropic media: Geophysics, **67**, 1564–1574.

Grechka, V., and I. Tsvankin, 1998, Feasibility of nonhyperbolic moveout inversion in transversely isotropic media: Geophysics, **63**, 957–969.

———, 1999, 3-D moveout velocity analysis and parameter estimation for orthorhombic media: Geophysics, **64**, 820–837.

———, 2002, PP + PS = SS: Geophysics, **67**, 1961–1971.

Grechka, V., I. Tsvankin, and J. Cohen, 1999, Generalized Dix equation and analytic treatment of normal-moveout velocity for anisotropic media: Geophysical Prospecting, **47**, 117–148.

Pech, A., and I. Tsvankin, 2004, Quartic moveout coefficient for a dipping azimuthally anisotropic layer: Geophysics, **69**, 699–707.

Schoenberg, M., and K. Helbig, 1997, Orthorhombic media: Modeling elastic wave behavior in a vertically fractured earth: Geophysics, **62**, 1954–1974.

Stork, C., 1992, Reflection tomography in the postmigrated domain: Geo-physics, **57**, 680–692.

Toldi, J., T. Alkhalifah, P. Berthet, J. Arnaud, P. Williamson, and B. Conche, 1999, Case study of estimation of anisotropy: The Leading Edge, **18**, 588–594.

Tsvankin, I., 1997, Anisotropic parameters and P-wave velocity for orthorhombic media: Geophysics, **62**, 1292–1309.

———, 2005, Seismic signatures and analysis of reflection data in anisotropic media, 2nd ed.: Elsevier.

Tsvankin, I., and L. Thomsen, 1994, Nonhyperbolic reflection moveout in anisotropic media: Geophysics, **59**, 1290–1304.

Van der Baan, M., and J.-M. Kendall, 2002, Estimating anisotropy parameters and traveltimes in the τ-p domain: Geophysics, **67**, 1076–1086.

———, 2003, Traveltime and conversion point computations and parameter estimation in layered anisotropic media by τ-p transform: Geophysics, **68**, 210–224.

Vasconcelos, I., and I. Tsvankin, 2006, Nonhyperbolic moveout inversion of wide-azimuth P-wave data for orthorhombic media: Geophysical Prospecting, **54**, 535–552.

Wang, Z., 2002, Seismic anisotropy in sedimentary rocks, Part 2: Laboratory data: Geophysics, **67**, 1423–1440.

Xu, X., and I. Tsvankin, 2006, Anisotropic geometrical-spreading correction for wide-azimuth P-wave reflections: Geophysics, **71**, no. 5, D161–D170.

———, 2007, A case study of azimuthal AVO analysis with anisotropic spreading correction: The Leading Edge, **26**, 1552–1561.